

Recent Results from the DØ Experiment

R. Dean Schamberger*

SUNY at Stony Brook - Dept of Physics & Astronomy
Stony Brook, New York - USA

This presentation reviews some of the recent results from the DØ experiment at the Tevatron proton-antiproton collider. Topics include W and Z boson properties, top quark properties, γ + heavy quark jets and searches for SUSY and the Higgs boson.

1 Introduction

In this talk I will present a sampling of recent results from the DØ experiment at the Tevatron. The best source of information on these measurements, many of which are preliminary, is on the DØ collaboration web page [2]. Also, there were a large number of parallel talks giving on DØ results at this conference which have more details on specific results.

The data presented here were taken with the DØ detector during the 2002-2008 running of the Tevatron collider at Fermilab, with proton-antiproton interactions at a center of mass energy of 1.96 TeV and have integrated luminosities of up to 4.3 fb^{-1} . The Tevatron has been performing well, delivering about 6.5 fb^{-1} , 2 fb^{-1} of which were accumulated in the last year alone.

The DØ detector [3] consists of tracking, calorimeter, and muon subdetector systems. Silicon microstrip tracking detectors (SMT) near the interaction point cover pseudorapidity $|\eta| \equiv -\ln(\tan(\theta/2)) \lesssim 3$ to provide tracking and vertex information. The central fiber tracker surrounds the SMT, providing coverage to $|\eta| \approx 2$. A 2 T solenoid surrounds these tracking detectors. Three uranium, liquid-argon calorimeters measure particle energies. The central calorimeter (CC) covers $|\eta| < 1.1$, and two end calorimeters (EC) extend coverage to $|\eta| \approx 4$. Muons are measured with stations which use scintillation counters and several layers of tracking chambers over the range $|\eta| < 2$. One such station is located just outside the calorimeters, with two more outside the 1.8 T iron toroidal magnets. Scintillators surrounding the exiting beams mounted on the face of both end calorimeters allow determination of the luminosity. A three level trigger system selects events for recording with a rate of 100 Hz.

2 Results

2.1 W Boson Mass

Knowledge of the W boson mass (m_W) is currently the limiting factor in our ability to tighten the constraints on the mass of the Higgs boson as determined from internal consistency of the standard model (SM) [4]. Improving the measurement of m_W is an important contribution to our understanding of the electroweak (EW) interaction, and, potentially, of how the electroweak symmetry is broken. The current world-average measured value of the W boson mass is $m_W = 80.399 \pm 0.025 \text{ GeV}$ [4] from a combination of measurements.

A measurement of the W boson mass using data collected from 2002 to 2006 with the DØ detector, corresponding to a total integrated luminosity of 1 fb^{-1} [5] with an average

*For the DØ collaboration

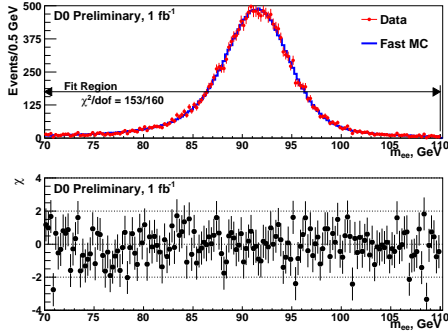


Figure 1: (top) The dielectron invariant mass distribution in $Z \rightarrow ee$ data and from the fast simulation (MC) and (bottom) the χ values where $\chi_i = (N_i - MC_i)/\sigma_i$ for each point in the distribution, N_i is the data yield in bin i and only the statistical uncertainty is used. The fit range is indicated by the double-ended horizontal arrow.

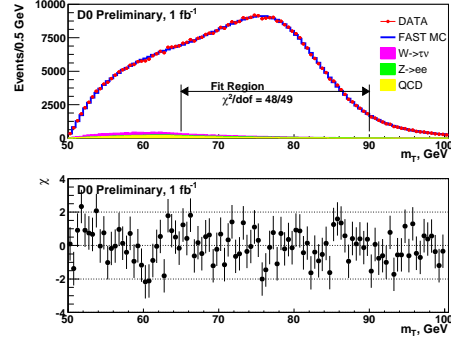


Figure 2: (top) The transverse mass distribution in $W \rightarrow e\nu$ data and from the fast simulation (MC) with backgrounds and (bottom) the χ values for the fit. The fit range is indicated by the double-ended horizontal arrow.

instantaneous luminosity of $41 \times 10^{30} \text{ cm}^{-2}\text{s}^{-1}$. We use the $W \rightarrow e\nu$ decay mode because the D0 calorimeter is well-suited for a precise measurement of electron energies, providing an energy resolution of 3.6% for electrons with an energy of 50 GeV. The components of the initial state total momentum and of the neutrino momentum along the beam direction are unmeasurable, so the W boson mass is measured using three kinematic variables measured in the plane perpendicular to the proton beam direction: the transverse mass m_T , the electron transverse momentum p_T^e , and the neutrino transverse momentum p_T^ν . The transverse mass is $m_T = \sqrt{2p_T^e p_T^\nu (1 - \cos \Delta\phi)}$, where $\Delta\phi$ is the opening angle between the electron and neutrino momenta in the plane transverse to the beam. The magnitude and direction of p_T^ν are inferred from the event missing transverse energy ($\vec{\cancel{p}}_T$). Candidate W boson events are required to have one cluster reconstructed in the CC, with $p_T^e > 25$ GeV and $|\eta_{\text{det}}| < 1.05$ where η_{det} is the pseudorapidity measured with respect to the center of the detector. The cluster must have one track matching it. The event must satisfy $\cancel{E}_T > 25$ GeV, $u_T < 15$ GeV, and $50 < m_T < 200$ GeV. Here u_T is the magnitude of the vector sum of the transverse component of the energies measured in calorimeter cells excluding those associated with the reconstructed electron. This selection yields 499,830 candidate $W \rightarrow e\nu$ events. We use $Z \rightarrow ee$ events for calibration. Candidate Z boson events are required to have two clusters satisfying the requirements above. Both electrons must have $p_T^e > 25$ GeV. The associated tracks must be of opposite charge. Events must also have $70 \text{ GeV} \lesssim m_{ee} \lesssim 110 \text{ GeV}$, where m_{ee} is the invariant mass of the dielectron pair. Events with both electrons in the CC are used to determine the EM calibration. There are 18,725 candidate $Z \rightarrow ee$ events in this category. Figure 1 shows the comparison between the fast MC and the data for the $Z \rightarrow ee$ events. Figure 2 shows the comparison between the fast MC and the data for the $W \rightarrow e\nu$ events using the m_T variable.

The systematic uncertainties in the W boson mass measurement arise from a variety of sources, and can be categorized as those from experimental sources and those from uncertainties in the production mechanism. The systematic uncertainties are summarized in Table 1. The largest uncertainty, 34 MeV arises from the precision with which the electron energy scale is known. This is limited by the statistical power of the $Z \rightarrow ee$ sample, and it is expected to improve with more data.

The m_W values extracted from fitting template distributions to the three kinematic variables m_T , p_T^e , and \cancel{E}_T are listed below.

$$\begin{aligned}
 m_W &= 80.401 \pm 0.023 \text{ (stat)} \pm 0.037 \text{ (syst)} \text{ GeV} = 80.401 \pm 0.044 \text{ GeV}(m_T) \\
 &= 80.400 \pm 0.027 \text{ (stat)} \pm 0.040 \text{ (syst)} \text{ GeV} = 80.400 \pm 0.048 \text{ GeV}(p_T^e) \text{ and} \\
 &= 80.402 \pm 0.023 \text{ (stat)} \pm 0.044 \text{ (syst)} \text{ GeV} = 80.402 \pm 0.050 \text{ GeV}(\cancel{E}_T).
 \end{aligned}$$

The results from the three methods have significant statistical correlations and the dominant systematic uncertainty is 100% correlated. Thus, although a combination is being performed, it is expected to have limited impact on the final uncertainty. The m_W value obtained from the transverse mass distribution using 1 fb^{-1} of data is shown in Figure 3 and is in good agreement with the current world average. Its introduction in global electroweak fits will lower the upper bound on the Standard Model Higgs mass, although it will not change the best fit value [4]. A Physical Review Letter is being written and should be submitted soon. More details on this analysis is available in a DØ conference note [6].

Source	σ MeV		
	m_T	p_T^e	\cancel{E}_T
Electron energy calibration	34	34	34
Electron resolution model	2	2	3
Electron energy offset	4	6	7
Electron energy loss model	4	4	4
Recoil model	6	12	20
Electron efficiencies	5	6	5
Backgrounds	2	5	4
Experimental Subtotal	35	37	41
PDF	10	11	11
QED	7	7	9
Boson p_T	2	5	2
Production Subtotal	12	14	14
Total	37	40	43

Table 1: Systematic uncertainties of the W boson mass measurement.

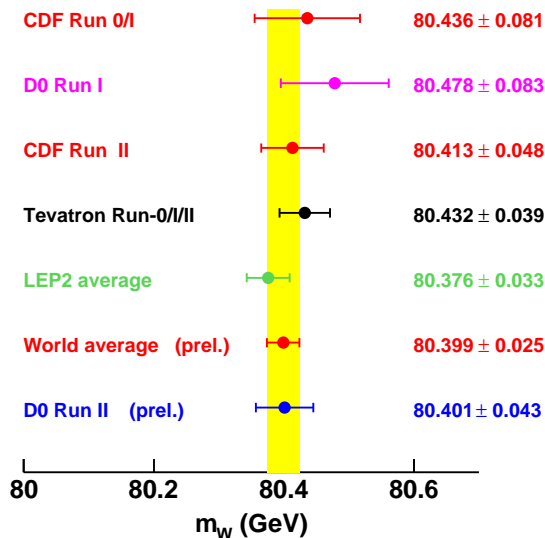


Figure 3: World Average W Boson Mass

2.2 W Boson Asymmetry

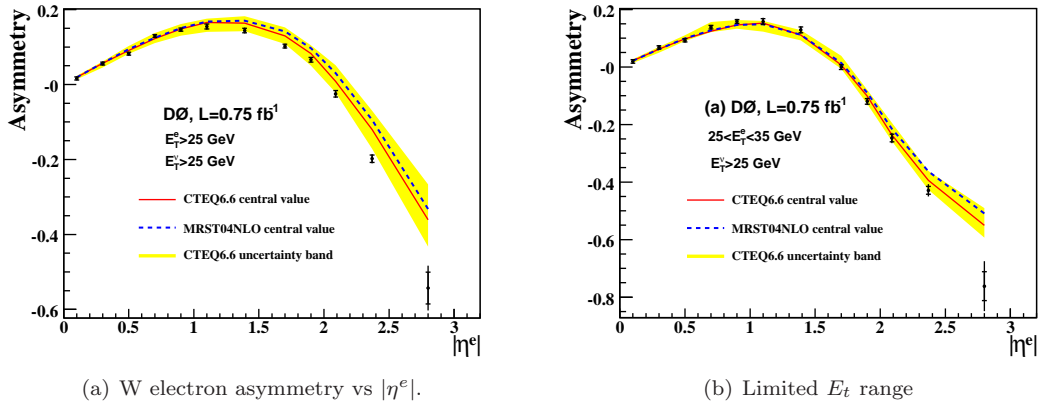


Figure 4: W electron asymmetry.

In proton-antiproton scattering, W^+ (W^-) bosons are produced primarily by the annihilation of u (d) quarks in the proton with \bar{d} (\bar{u}) quarks in the antiproton. Any difference between the u - and d -quark parton distribution functions (PDFs) will result in an asymmetry in the W boson rapidity distribution between W^+ and W^- boson production. We detect W bosons via their decay $W \rightarrow e\nu$. The boson rapidity (y_W) can not be measured due to the unknown longitudinal momentum of the neutrino. We instead measure the electron charge asymmetry, which is a convolution of the W boson production asymmetry and the parity violating asymmetry from the W boson decay. Since the V-A interaction is well understood, the lepton charge asymmetry retains sensitivity to the underlying W boson asymmetry. The electron selection criteria is similar to the W mass analysis, except that the acceptance is extended to $|\eta^e| < 3.2$ using 0.75 fb^{-1} of data. The charge asymmetry is measured in 24 electron pseudorapidity bins and two electron E_T bins. Figure 4a shows the folded electron charge asymmetry compared to theoretical predictions. Figure 4b shows the lower of the two E_T bins. Our result [7] can be used to improve the precision and accuracy of next generation PDF sets, and will help to reduce the PDF uncertainty for high precision M_W measurements

2.3 Photons plus Heavy Quark Jets

Photons (γ) produced in association with heavy quarks Q ($\equiv c$ or b) in the final state of hadron-hadron interactions provide valuable information about the parton distributions of the initial state hadrons. Such events are produced primarily through the QCD Compton-like scattering process $gQ \rightarrow \gamma Q$, which dominates up to photon transverse momenta (p_T^γ) of ≈ 90 GeV for $\gamma+c+X$ and up to ≈ 120 GeV for $\gamma+b+X$ production, but also through quark-antiquark annihilation $q\bar{q} \rightarrow \gamma g \rightarrow \gamma Q\bar{Q}$. Consequently, $\gamma+Q+X$ production is sensitive to the b , c , and gluon (g) densities within the colliding hadrons, and can provide constraints on parton distribution functions (PDFs) that have substantial uncertainties. The heavy quark and gluon content is an important aspect of QCD dynamics and of the fundamental structure of the proton. In particular, many searches for new physics, e.g. for certain Higgs boson

production modes, will benefit from a more precise knowledge of the heavy quark and gluon content of the proton.

DØ has performed the first measurement [8] of the differential cross section of inclusive photon production in association with heavy flavor (b and c) jets at a $p\bar{p}$ collider. The results cover the range $30 < p_T^\gamma < 150$ GeV, $|y^\gamma| < 1.0$, and $|y^{\text{jet}}| < 0.8$. The measured cross sections provide information about b , c , and gluon PDFs for $0.01 \leq x \leq 0.3$. NLO pQCD predictions using cteq6.6M PDFs for $\gamma+b+X$ production agree with the measurements over the entire p_T^γ range. We observe disagreement between theory and data for $\gamma+c+X$ production for $p_T^\gamma > 70$ GeV (see Figure 5).

2.4 $Z + \gamma \rightarrow \nu\bar{\nu} + \gamma$

The standard model (SM) of electroweak interactions is described by the non-Abelian gauge group $SU(2) \times U(1)$. The symmetry transformations of the group allow interactions involving three gauge bosons (γ , W , and Z) through trilinear gauge boson couplings. However, the SM forbids such vertices for the photon and the Z boson at the lowest *tree* level, i.e., the values of the $Z\gamma\gamma$ and $ZZ\gamma$ couplings vanish. The cross section for the SM $Z\gamma$ production is very small.

However, the presence of finite (anomalous) $Z\gamma\gamma$ and $ZZ\gamma$ couplings can enhance the yields, especially at higher values of the photon transverse energy (E_T). The observation of an anomalously high $Z\gamma$ production rate could, therefore, indicate the presence of new physics.

Data for this analysis were collected with the DØ detector in the period from 2002 to 2008, and correspond to an integrated luminosity of 3.6 fb^{-1} . We obtain the photon sample by selecting events with a single photon candidate of $E_T > 90$ GeV and $|\eta| < 1.1$, and require a missing transverse energy in the event of $\cancel{E}_T > 70$ GeV, which effectively suppresses the multijet background.

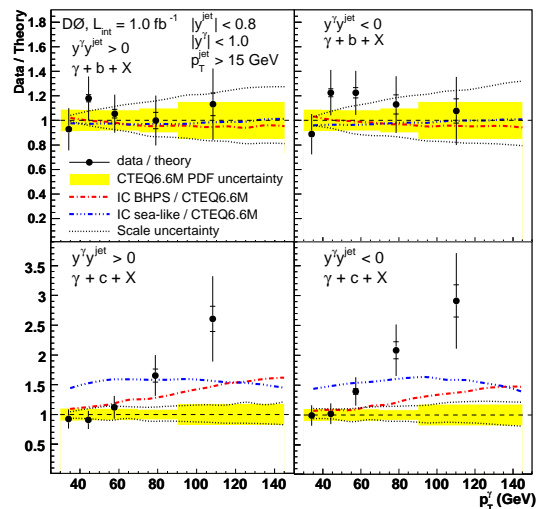


Figure 5: The data-to-theory ratio of cross sections as a function of p_T^γ for $\gamma+b+X$ and $\gamma+c+X$ in the regions $y^\gamma y^{\text{jet}} > 0$ and $y^\gamma y^{\text{jet}} < 0$. The uncertainties on the data include both statistical (inner line) and full uncertainties (entire error bar). Also shown are the uncertainties on the theoretical pQCD scales and the cteq6.6M PDFs. The scale uncertainties are shown as dotted lines and the PDF uncertainties by the shaded regions.

	Number of events
$W \rightarrow e\nu$	$9.67 \pm 0.30(\text{stat.}) \pm 0.48(\text{syst.})$
non-collision	$5.33 \pm 0.39(\text{stat.}) \pm 1.91(\text{syst.})$
W/Z + Jets	$1.37 \pm 0.26(\text{stat.}) \pm 0.91(\text{syst.})$
$W\gamma$	$0.90 \pm 0.07(\text{stat.}) \pm 0.12(\text{syst.})$
Total background	$17.3 \pm 0.6(\text{stat.}) \pm 2.3(\text{syst.})$
$N_{\nu\bar{\nu}\gamma}^S M$	33.7 ± 3.4
N_{obs}	51

Table 2: Summary of background estimates, and the number of observed and SM predicted events.

To minimize large \cancel{E}_T from mismeasurement of jet energy, we reject events with jets with $E_T > 15$ GeV. After applying all selection criteria, we observe 51 candidate events with a predicted background of $17.3 \pm 0.6(\text{stat.}) \pm 2.3(\text{syst.})$ events. The summary of backgrounds is shown in Table 2. The $Z\gamma$ cross section multiplied by the branching fraction of $Z \rightarrow \nu\bar{\nu}$ is measured to be $32 \pm 9(\text{stat.} + \text{syst.}) \pm 2(\text{lumi.})$ fb [9] for the photon $E_T > 90$ GeV, which is in good agreement with the NLO cross section of 39 ± 4 fb. To set limits on the ATGC, we compare the photon E_T spectrum in data with that from the sum of expected $Z\gamma$ signal and the background (see Figure 6) for each pair of couplings for a grid in which h_{30}^V runs from -0.12 to 0.12 with a step of 0.01, and h_{40}^V varies from -0.08 to 0.08 with a step of 0.001. The MC samples are generated with the LO $Z\gamma$ generator (corrected for the NLO effects with an E_T -dependent K-factor) for the form-factor $\Lambda = 1.5$ TeV.

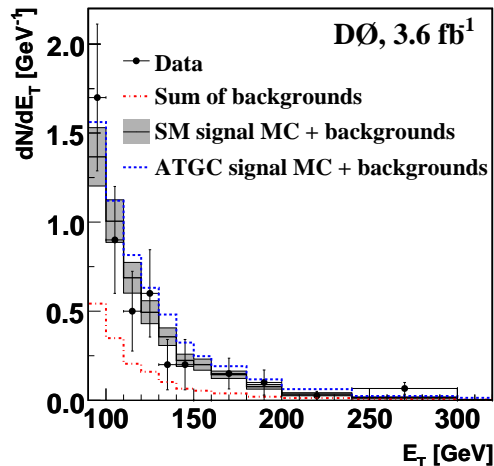


Figure 6: Photon E_T spectrum in data (solid circles), sum of backgrounds (dash-dot line), and sum of MC signal and background for the SM prediction (solid line) and for the ATGC prediction with $h_{30}^\gamma = 0.09$ and $h_{40}^\gamma = 0.005$ (dashed line). The shaded band corresponds to the ± 1 s.d. total uncertainty on the predicted sum of SM signal and background.

2.5 Top Quark Mass

DØ has recently combined the best DØ measurements from Run I of the Tevatron in the dilepton [10] and lepton+jets [11] channels, and the most recent Run II measurements in the dilepton [12] and the lepton+jets [13] channels with 3.6 fb^{-1} data set. We use the BLUE [14] method to perform the combination of the top quark mass measurements. We follow the same procedure, use the same classes of uncertainties and the same package as is used to compute the world average top quark mass.

Combining the top quark mass measurements performed using Run IIa and Run IIb data in γ +jets channel we obtain:

$$\begin{aligned} m_{\text{top}}^{\ell+\text{jets}} &= 173.7 \pm 0.8 (\text{stat}) \pm 1.6 (\text{syst}) \text{ GeV} \\ &= 173.7 \pm 1.8 \text{ GeV}. \end{aligned}$$

The χ^2 for the combination is 2.5 for 1 degree of freedom. The probability to get this or larger value of the χ^2 is 11.2%. The combined top quark mass measurement in the dilepton channel using up to 3.6 fb^{-1} of data in ee, $e\mu$, $\mu\mu$ and lepton+track channels is:

$$\begin{aligned} m_{\text{top}}^{\ell\ell} &= 174.7 \pm 2.9 (\text{stat}) \pm 2.4 (\text{syst}) \text{ GeV} \\ &= 174.7 \pm 3.8 \text{ GeV}. \end{aligned}$$

Combination of all Run I and Run II measurements (see Figure 7) yields:

$$\begin{aligned} m_{\text{top}} &= 174.2 \pm 0.9 \text{ (stat)} \pm 1.5 \text{ (syst)} \text{ GeV} \\ &= 174.2 \pm 1.7 \text{ GeV.} \end{aligned}$$

For more details on the combination see the DØ conference note [15].

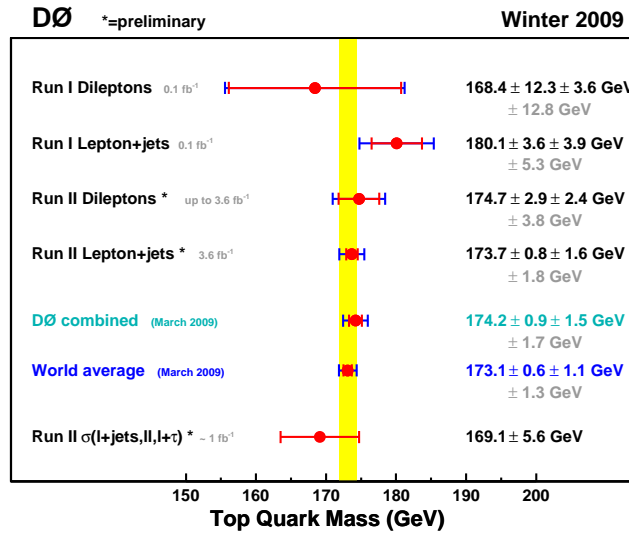


Figure 7: A summary of the top quark mass measurements used for the DØ combination along with the DØ combination results, and the world average top quark mass.

2.6 Single Top Production

Single top quark production serves as a probe of the Wtb interaction, and its production cross section provides a direct measurement of the magnitude of the quark mixing matrix element V_{tb} without assuming three quark generations. However, measuring the yield of single top quarks is difficult because of the small production rate and large backgrounds. When top quarks are produced singly, they are accompanied by a bottom quark in the s-channel production mode or by both a bottom quark and a light quark in t-channel production, as illustrated in Figure 8. We search for both of these processes at once. The sum of their predicted cross sections is 3.46 ± 0.18 pb for a top quark mass $m_t = 170$ GeV.

The measurement focuses on the final state containing one high transverse momentum lepton ($\ell = \text{electron or muon}$) not near a jet (*isolated*), large missing transverse energy (\cancel{E}_T)

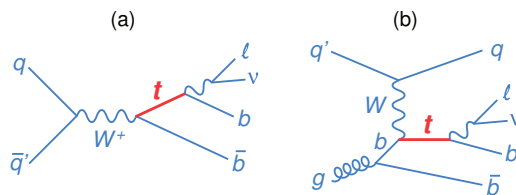


Figure 8: Representative Feynman diagrams for (a) s-channel single top quark production and (b) t-channel production, showing the top quark decays of interest.

indicative of the passage of a neutrino ν , a b-quark jet from the decay of the top quark ($t \rightarrow Wb \rightarrow \ell\nu b$), and possibly another b jet and a light jet as indicated above.

Three multivariate techniques use the same data sample but are not completely correlated. Their combination therefore leads to increased sensitivity and a more precise measurement of the cross section. We use the three discriminant outputs as inputs to a second set of Bayesian neural networks, and obtain the combined cross section and its signal significance from the new discriminant output. The resulting expected significance is 4.5 SD. Figure 9 illustrates the importance of the signal when comparing data to prediction. The measured cross section is $\sigma(p\bar{p} \rightarrow tb + X, tqb + X) = 3.94 \pm 0.88$ pb. The measurement has a p-value of 2.5×10^{-7} , corresponding to a significance of 5.0 SD. The expected and measured posterior densities are shown in Fig. 10.

We use the cross section measurement to determine the Bayesian posterior for $|V_{tb}|^2$ in the interval $[0,1]$ and extract a limit of $|V_{tb}| > 0.78$ at 95% C.L. within the SM. When the upper constraint is removed, we measure $|V_{tb}f_1^L| = 1.07 \pm 0.12$, where f_1^L is the strength of the left-handed Wtb coupling. For more details on these results see reference [16].

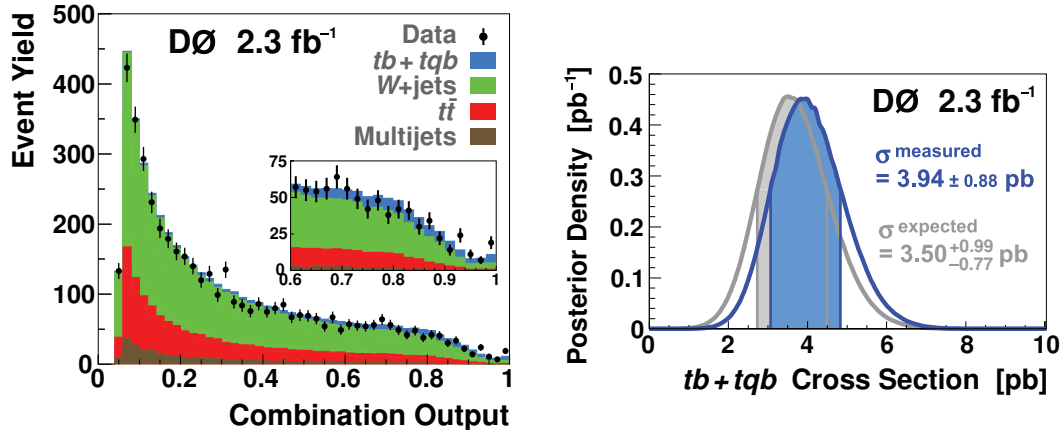


Figure 9: Distribution of the combination output for all analysis channels combined. The signal is normalized to the measured cross section.

Figure 10: Expected SM and measured Bayesian posterior probability densities for the $tb + tqb$ cross section. The shaded regions indicate one standard deviation above and below the peak positions.

3 Searches

3.1 SUSY in Tri-lepton final states

The $D\bar{O}$ experiment has new results of a search for associated production of charginos and neutralinos using a data set corresponding to an integrated luminosity of 2.3 fb^{-1} collected during Run II of the Tevatron proton-antiproton collider. Final states containing three charged leptons and missing transverse energy are probed for a signal from supersymmetry with four dedicated trilepton event selections. No evidence for a signal is observed, and we set limits on the product of production cross section and leptonic branching fraction.

Within minimal supergravity, these limits translate into bounds on m_0 and $m_{1/2}$ that are well beyond existing limits.

In this analysis four different channels are defined, distinguished by the lepton content of the final state. For the di-electron plus lepton channel ($ee\ell$) two identified electrons are required. In the di-muon plus lepton channel ($\mu\mu\ell$), one tight and one loose muon are required, while the selection in the electron, muon plus lepton channel ($e\mu\ell$) starts from one electron and one tight muon. Finally, the muon, τ lepton plus lepton channel ($\mu\tau\ell$) requires one tight muon and one hadronically decaying τ lepton in the final state. The third lepton is reconstructed as an isolated track without using the standard lepton identification criteria [17].

Figure 11 shows the region excluded in the m_0 - $m_{1/2}$ plane for $\tan\beta=3$, $A_0=0$ and $\mu > 0$ in comparison with the limits from chargino and slepton searches at LEP [18] and CDF [19]. The shape of the excluded region is driven by the relation of gaugino and slepton masses throughout the plane, which affects the branching fraction into three charged leptons as well as the efficiencies of the selections.

Figure 12 shows the limit on $\sigma \times \text{BR}(3\ell)$ as a function of $\tan\beta$ for a chargino mass of 130 GeV and fixing m_0 such that the lightest stau ($\tilde{\tau}_1$) is heavier than the $\tilde{\chi}_2^0$ by 1 GeV. The latter choice results in three-body decays with maximal leptonic branching fraction.

3.2 Higgs

Despite its success as a predictive tool, the standard model of particle physics remains incomplete without a means to explain electroweak symmetry breaking. The simplest proposed mechanism involves the introduction of a complex doublet of scalar fields that generate the masses of elementary particles via their mutual interactions. After accounting for longitudinal polarizations for the electroweak bosons, this so-called Higgs mechanism also gives rise to a single scalar

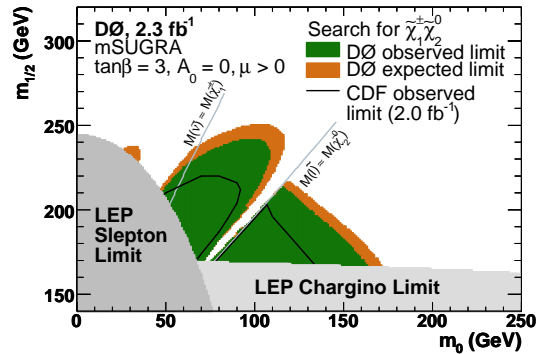


Figure 11: Region in the m_0 vs $m_{1/2}$ plane excluded by the combination of the $D\bar{O}$ analyses (green), by LEP searches for charginos (light gray) and sleptons (dark gray) and CDF (black line). The assumed mSUGRA parameters are $\tan\beta=3$, $A_0=0$ and $\mu > 0$.

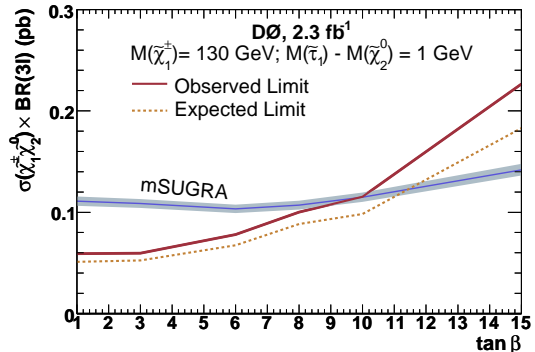


Figure 12: Upper limit at the 95% C.L. on $\sigma \times \text{BR}(3\ell)$ as a function of $\tan\beta$ in comparison with the prediction for a chargino mass of 130 GeV and $m_{\tilde{\tau}_1} - m_{\tilde{\chi}_2^0} = 1$ GeV.

boson with an unpredicted mass. Direct searches in $e^+e^- \rightarrow Z^* \rightarrow ZH$ at the LEP collider yielded lower mass limits at $m_H > 114.4$ GeV while precision electroweak data yield the indirect constraint $m_H < 154$ GeV, with both limits set at 95% confidence level (C.L.). When also considering the direct limit, the indirect constraint predicts $m_H < 185$ GeV, indicating that the range $110 \leq m_H \leq 200$ GeV is the most important search region for a SM Higgs boson. The search for a SM Higgs boson is one of the main goals of the Fermilab Tevatron physics program.

Searches for standard model Higgs boson production with the DØ detector in $p\bar{p}$ collisions at $\sqrt{s} = 1.96$ TeV have been carried out for Higgs boson masses (m_H) in the range $100 < m_H < 200$ GeV. The contributing production processes include associated production ($q\bar{q} \rightarrow W/ZH$), gluon fusion ($gg \rightarrow H$), and vector boson fusion ($q\bar{q} \rightarrow q'\bar{q}'H$). Analyses are conducted with integrated luminosities from 0.9 fb^{-1} to 4.2 fb^{-1} . As no significant excess is observed, we proceed to set limits on standard model Higgs boson production. The observed 95% confidence level upper limits are found to be a factor of 3.7 (1.3) higher than the predicted standard model cross section at $m_H = 115$ (165) GeV while the expected limits are found to be a factor of 3.6 (1.7) higher than the standard model cross section for the same masses. The 59 analyses used in this combination are outlined in Table 3. In

Channel	Data Epoch	Luminosity (fb^{-1})	Final Variable	# Sub-Channels
$WH \rightarrow \ell\nu b\bar{b}$, ST/DT, $W+2$ jet	Run IIa+Run IIb	2.7	NN discriminant	8
$WH \rightarrow \ell\nu b\bar{b}$, ST/DT, $W+3$ jet	Run IIa+Run IIb	2.7	Dijet Mass	8
$WH \rightarrow \tau\nu b\bar{b}$	Run IIa	0.9	Dijet Mass	5
$H+X \rightarrow \tau\tau b\bar{b}/q\bar{q}\tau\tau$	Run IIa	1.0	NN discriminant	1
$ZH \rightarrow \nu\bar{\nu} b\bar{b}$, DT	Run IIa+Run IIb	2.1	DTree discriminant	2
$ZH \rightarrow e^+e^- b\bar{b}$, ST/DT	Run IIa	1.1	NN discriminant	2
$ZH \rightarrow \mu^+\mu^- b\bar{b}$, ST/DT	Run IIa	1.1	DTree discriminant	2
$ZH \rightarrow e^+e^- b\bar{b}$, ST/DT	Run IIb	3.1	DTree discriminant	6
$ZH \rightarrow \mu^+\mu^- b\bar{b}$, ST/DT	Run IIb	3.1	DTree discriminant	2
$ZH \rightarrow \mu^\pm + \text{track } b\bar{b}$, ST/DT	Run IIa+Run IIb	4.2	DTree discriminant	2
$WH \rightarrow WW^+W^-$	Run IIa	1.1	2-D Likelihood	3
$WH \rightarrow WW^+W^-$	Run IIb	2.5	1-D Likelihood	3
$H \rightarrow W^+W^- (\mu^+\mu^-)$	Run IIa+Run IIb	3.0	NN discriminant	1
$H \rightarrow W^+W^- (e^\pm\mu^\mp)$	Run IIa+Run IIb	4.2	NN discriminant	1
$H \rightarrow W^+W^- (e^+e^-)$	Run IIa+Run IIb	4.2	NN discriminant	1
$H \rightarrow \gamma\gamma$	Run IIa+Run IIb	4.2	Di-photon Mass	1
$t\bar{t}H \rightarrow t\bar{t}b\bar{b}$	Run IIa+Run IIb	2.1	Scaled H_T	12

Table 3: List of channels and luminosities used in the DØ combined Higgs search.

the cases of $p\bar{p} \rightarrow W/ZH + X$ production, we search for a Higgs boson decaying to two bottom quarks. We also consider Higgs decays to two W^\pm bosons. For $WH \rightarrow WW^+W^-$ production, we search for leptonic W boson decays with three final states of two same-signed leptons: $WWW \rightarrow e^\pm\nu e^\pm\nu + X$, $e^\pm\nu\mu^\pm\nu + X$, and $\mu^\pm\nu\mu^\pm\nu + X$. In the case of $p\bar{p} \rightarrow H \rightarrow W^+W^-$ and $p\bar{p} \rightarrow q\bar{q}H \rightarrow q\bar{q}W^+W^-$ production via vector boson fusion, we search for leptonic W boson decays with three final states of opposite-signed leptons: $WW \rightarrow e^+\nu e^-\nu, e^\pm\nu\mu^\mp\nu$, and $\mu^+\nu\mu^-\nu$. For the gluon fusion and vector boson fusion processes, $H \rightarrow b\bar{b}$ decays are not considered due to the large multijet background. In all $H \rightarrow W^+W^-$ decays with $m_H < 2M_W$, one of the W bosons will be off mass shell. In all cases, lepton selections include both electrons and muons ($\ell = e, \mu$), but τ leptons

are included in the simulation and the selections necessarily have acceptance for secondary leptons from $\tau \rightarrow e\nu, \mu\nu$ decays. Finally, we include an analysis that searches for Higgs bosons decaying to two photons and produced via gluon-gluon fusion, vector boson fusion, and associated production mechanisms.

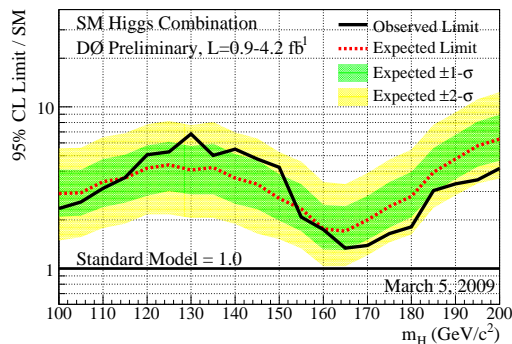


Figure 13: $D\bar{O}$ expected (median, for the background-only hypothesis) and observed 95% C.L. cross section upper limit ratios to the SM for the combined analyses over the $100 \leq m_H \leq 200$ GeV mass range. The limits are evaluated for test masses every 5 GeV. The points are joined by straight lines for better readability. The bands indicate the 68% and 95% probability regions where the limits can fluctuate, in the absence of signal.

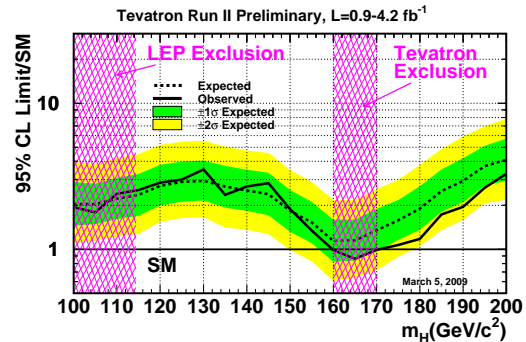


Figure 14: Observed and expected (median, for the background-only hypothesis) 95% C.L. upper limits on the ratios to the SM cross section, as functions of the Higgs boson mass for the combined CDF and $D\bar{O}$ analyses. The limits are expressed as a multiple of the SM prediction for test masses (every 5 GeV) for which both experiments have performed dedicated searches in different channels. The points are joined by straight lines for better readability. The bands indicate the 68% and 95% probability regions where the limits can fluctuate, in the absence of signal.

Figure 13 shows the expected and observed 95% C.L. cross section limit ratio to the SM cross sections for all $D\bar{O}$ analyses combined over the probed mass region ($100 \leq m_H \leq 200$ GeV). For more details on this combination see the $D\bar{O}$ conference note [20]. In addition the TEVNP Working Group have combined the results from CDF and $D\bar{O}$ on direct searches for a standard model Higgs boson in $p\bar{p}$ collisions at the Fermilab Tevatron at $\sqrt{s} = 1.96$ TeV. With $2.0\text{-}3.6 \text{ fb}^{-1}$ of data analyzed at CDF, and $0.9\text{-}4.2 \text{ fb}^{-1}$ at $D\bar{O}$, the 95% C.L. upper limits on Higgs boson production are a factor of 2.5 (0.86) times the SM cross section for a Higgs boson mass of $m_H = 115$ (165) GeV. Based on simulation, the corresponding median expected upper limits are 2.4 (1.1). The mass range excluded at 95% C.L. for a SM Higgs has been extended from earlier combinations to $160 < m_H < 170$ GeV. The ratios of the 95% C.L. expected and observed limit to the SM cross section are shown in figure 14. For more details on this combination see the Fermilab note [21].

Acknowledgments

We thank the staffs at Fermilab and collaborating institutions, and acknowledge support from the DOE and NSF (USA); CEA and CNRS/IN2P3 (France); FASI, Rosatom and RFBR (Russia); CNPq, FAPERJ, FAPESP and FUNDUNESP (Brazil); DAE and DST (India); Colciencias (Colombia); CONACyT (Mexico); KRF and KOSEF (Korea); CONICET and UBACyT (Argentina); FOM (The Netherlands); STFC and the Royal Society (United Kingdom); MSMT and GACR (Czech Republic); CRC Program, CFI, NSERC and WestGrid Project (Canada); BMBF and DFG (Germany); SFI (Ireland); The Swedish Research Council (Sweden); CAS and CNSF (China); and the Alexander von Humboldt Foundation (Germany).

References

- [1] Slides:
<http://indico.cern.ch/contributionDisplay.py?contribId=4&sessionId=7&confId=53294>
- [2] <http://www-d0.fnal.gov/Run2Physics/WWW/results.htm>
- [3] V.M. Abazov *et al.* (DØ Collaboration), Nucl. Instrum. Methods in Phys. Res.A **565**, 463 (2006).
- [4] The LEP Electroweak Working Group, CERN-PH-EP/2008-20, arXiv:0811.4682 [hep-ex] (2008), and The Tevatron Electroweak Working Group, FERMILAB-TM-2415. More information is available at: <http://tevewwg.fnal.gov>.
- [5] T. Andeen *et al.*, Fermilab Report No. FERMILAB-TM-2365.
- [6] V. M. Abazov *et al.* [DØ Collaboration], DØ note 5893-CONF (2009).
- [7] V. M. Abazov *et al.* [DØ Collaboration], Phys. Rev. Lett. **101**, 211801 (2008) [arXiv:0807.3367 [hep-ex]].
- [8] V. M. Abazov *et al.* [DØ Collaboration], Phys. Rev. Lett. **102**, 192002 (2009) [arXiv:0901.0739 [hep-ex]].
- [9] V. M. Abazov *et al.* [DØ Collaboration], Phys. Rev. Lett. **102**, 201802 (2009) [arXiv:0902.2157 [hep-ex]].
- [10] B. Abbott *et al.* [DØ Collaboration], Phys. Rev. Lett. **80**, 2063 (1998), B. Abbott *et al.* [DØ Collaboration], Phys. Rev. D **60**, 052001 (1999).
- [11] V. M. Abazov *et al.* [DØ Collaboration], Nature **429**, 638 (2004).
- [12] V. M. Abazov *et al.* [DØ Collaboration], Submitted to Phys. Rev. D, arXiv:0904.3195 [hep-ex], V. M. Abazov *et al.* [DØ Collaboration], DØ note 5897-CONF (2009).
- [13] V. M. Abazov *et al.* [DØ Collaboration], Phys. Rev. Lett. **101**, 182001 (2008) [arXiv:0807.2141 [hep-ex]], V. M. Abazov *et al.* [DØ Collaboration], DØ note 5877-CONF (2009).
- [14] L. Lyons, D. Gibout, and P. Clifford, Nucl. Instrum. Meth. A **270**, 110 (1988) and A. Valassi, Nucl. Instrum. Meth. A **500**, 391 (2003).
- [15] V. M. Abazov *et al.* [DØ Collaboration], DØ note 5900-CONF (2009).
- [16] V. M. Abazov *et al.* [DØ Collaboration], Submitted to Phys. Rev. Lett., arXiv:0903.0850 [hep-ex].
- [17] V. M. Abazov *et al.* [DØ Collaboration], Submitted to Phys. Lett. B, arXiv:0901.0646 [hep-ex].
- [18] LEPSUSYWG, ALEPH, DELPHI, L3 and OPAL Collaborations, notes LEPSUSYWG/01-03.1 and 04-01.1 (<http://lepsusy.web.cern.ch/lepsusy/Welcome.html>).
- [19] T. Aaltonen *et al.* [CDF Collaboration], Phys. Rev. Lett. **101**, 251801 (2008) [arXiv:0808.2446 [hep-ex]].
- [20] V. M. Abazov *et al.* [DØ Collaboration], DØ note 5902-CONF (2009).
- [21] The TEVNPH Working Group [CDF and DØ Collaborations], Fermilab-PUB-09-060-E (2009).